

# Study of concentration-dependent quantum yield of Rhodamine 6G by gold nanoparticles using thermal-lens technique

B. Rajesh Kumar · N. Shemeena Basheer ·  
Achamma Kurian · Sajan D. George

Received: 20 May 2013 / Accepted: 7 August 2013 / Published online: 17 August 2013  
© Springer-Verlag Berlin Heidelberg 2013

**Abstract** Tailoring optical properties of the dye molecules using metal nanoparticles is a burgeoning area of research. In this work, we report our results on the studies of how the absorption and emission behavior of Rhodamine 6G dye is tailored using gold nanoparticles. Furthermore, the influence of dye concentration on these properties for a given concentration of nanoparticles in the dye-nanoparticle mixture is investigated. In addition, the difference between the concentration-dependent fluorescence quantum yield of the dye molecules is measured in the absence and presence of nanoparticles using the dual-beam thermal-lens technique. Our absorption spectral studies show additional spectral features due to nanoparticle aggregation on interaction with cationic Rhodamine 6G dye. Dye concentration-dependent steady-state fluorescence studies in the presence of nanoparticles indicate a blue shift in peak fluorescence emission wavelength. The quantum yield value measured using thermal-lens technique exhibit a non-monotonic behavior with dye concentration with substantial quenching for lower dye concentrations. The results are interpreted in terms of dye–nanoparticle interaction and the formation of dye shell around the nanoparticle.

## 1 Introduction

Metal nanoparticles (MNPs) that exhibit rich plasmonic resonance properties due to collective electron oscillations of electrons in the visible range have been extensively used to tailor the properties of organic molecules. This kind of interactions find wide applications in diverse fields such as surface enhanced Raman spectroscopy [1, 2], plasmon enhanced fluorescence [3] and nanoscale lasers [4]. Interaction of NPs with organic dye molecules has been an important research area in the field of photonics. It is reported that the NP can either enhance or quench the intrinsic luminescence of an emitter, depending upon the emitter-donor distance. The fluorescence enhancement is normally attributed to the plasmon field generated around the NP by the incident light. This plasmon field can cause an increase in excitation decay rate with a concomitant increase in radiative quantum efficiency. On the other hand, the dipole energy around the nanoparticle reduces the ratio of the radiative to non-radiative decay rate via energy transfer mechanism resulting in the quenching of intrinsic fluorescence of the dye molecule [5]. Thus, the fluorescence quantum yield (FQY), which is the fraction of emitted light to the absorbed light by the dye molecule, can be tailored by mixing it with solution containing NPs. The measurement of fluorescence signal from a reference sample is a prerequisite for the evaluation of absolute FQY value of the dye. However, conventional fluorescence method suffers from the limitations such as availability of small number of standard samples, error in the absolute value of FQY of the reference sample, differences in refractive index, polarization effects, differences in wavelength response of monochromators and detectors and inner-filter effects [6]. Moreover, for the accurate determination of

B. R. Kumar · N. S. Basheer · A. Kurian  
Photonics Lab, Department of Physics, Catholicate College,  
Pathanamthitta 689645, India

S. D. George (✉)  
Centre for Atomic and Molecular Physics, Manipal University,  
Manipal 576104, Karnataka, India  
e-mail: sajan.george@manipal.edu

FQY, we have to consider both radiative as well as non-radiative processes occurring in the medium. In this context, employment of the photothermal techniques such as thermal-lens (TL) technique is proposed as an efficient approach to measure FQY. Compared to conventional fluorescence based approaches, the TL technique measures the photon energy that is converted into heat. As a consequence, TL technique depends only upon the absorbed light and is free from scattering. In addition, this technique is sensitive to absorption coefficient as low as  $10^{-7} \text{ cm}^{-1}$ . Moreover, TL that probe non-radiative channel of de-excitation can act as a complementary approach to conventional steady-state fluorescence methods that follow radiative path of deexcitation. It has been already demonstrated that TL technique can be effectively employed to determine the absolute FQY, molecular distance, energy transfer and two-photon absorption in photonic materials [7–17].

We report here the results of the experiments that we have carried out to probe how the presence of gold nanoparticle (AuNP) influences the emission behavior of Rhodamine 6G (Rh6G). Furthermore, we investigate the dye concentration-dependent absorption, emission, shift in fluorescence peak and the quantum yield of Rh6G in the presence of fixed concentration of Au NP. Our results show that the adsorption of dye molecules around the NP determines the emission characteristics of the dye-NP mixtures. Being an extensively used dye for lasing action as well as in surface enhanced Raman spectroscopy, the present study has great practical and physical significance.

## 2 Experimental procedure

### 2.1 Preparation of gold nanoparticles

In order to prepare the AuNPs, we followed the procedure explained elsewhere [18]. All the reagents used are of AR grade. Chloroauric acid ( $\text{HAuCl}_4 \cdot 3\text{H}_2\text{O}$ , 99.9%) and sodium citrate tribasic dihydrate ( $\text{C}_6\text{H}_5\text{Na}_3\text{O}_7$ , 99.99%) purchased from Sigma-Aldrich are used as received. Double-distilled water is used throughout the course of this preparation. In brief, the procedure followed is as follows; initially, 100 ml of 1 mM  $\text{HAuCl}_4 \cdot 3\text{H}_2\text{O}$  is heated to boiling, refluxed while being stirred. Then 10 ml of a 38.8 mM trisodium citrate solution is added quickly. The solution color changed from yellow to black and then to deep red indicating the formation of AuNPs. The size of the NPs is controlled by the amount of citrate solution in the mixture.

### 2.2 Preparation of samples for quantum yield measurements

An accurately weighed amount of Rh6G (Sigma-Aldrich, dye content 99.99 %) is dissolved in double-distilled water to give a concentration of  $10^{-3} \text{ M}$ . From this stock solution, sample solutions with different concentrations ranging from  $0.3 \times 10^{-5}$  to  $0.3 \times 10^{-3} \text{ M}$  are prepared. Rh6G dye molecule is reported to exhibit high quantum yield value ( $\sim 0.95$ ) for low concentration and exhibit self-quenching of the fluorescence at higher concentrations [14]. The maximum value of the concentration employed here is limited by nearly complete self-quenching of the dye molecule fluorescence. In order to investigate the influence of AuNPs on fluorescence emission behavior of Rh6G at different concentrations, 0.5 nM of Au nanofluid is mixed with various concentrations of Rh6G.

### 2.3 Quantum yield measurement setup

The dual-beam TL setup employed for the FQY measurement is shown in Fig. 1. Laser radiation at 532 nm wavelength from a diode-pumped solid-state laser (Coherent Inc. 20 mW) is used as the pump beam to generate the TL in the medium. Radiation of wavelength 632 nm from a low-power intensity stabilized He–Ne laser (Melles-Griot 1 mW) source is used as the probe beam. The pump beam is intensity modulated at 6 Hz using a mechanical chopper (Stanford Research Systems SR 530). Sample in the cuvette is kept in the pump beam path. The probe beam is made to pass collinearly through the sample using a dichroic mirror. A filter is placed in the path of the emergent beams which allows only the 632 nm wavelength to pass through it. An optical fiber mounted on an X–Y–Z translator is used to couple the probe beam to a monochromator–photomultiplier tube (PMT) assembly. The signal output from the PMT is processed using a dual phase lock-in amplifier (SR 830).

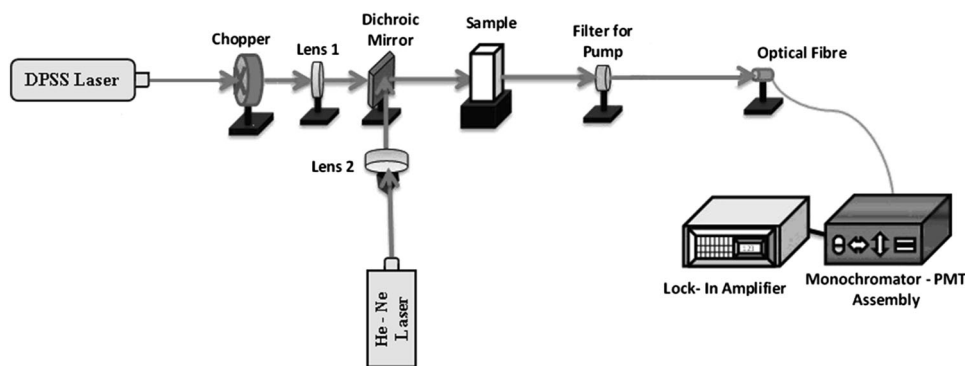
## 3 Theory

Fluorescence quantum yield of materials can be evaluated based on the principle of energy conversion. Let  $P_L$  be the power of the incident pump beam and  $P_t$  the power of the transmitted beam. The absorbed power is the sum of the laser power degraded to heat,  $P_{th}$  and luminescence emission  $P_f$ , provided that no photochemical reaction occurs [14]. Hence,

$$P_L = P_{th} + P_f + P_t \quad (1)$$

where it is assumed that the reflection and scattering losses are negligibly small [14].

**Fig. 1** Schematic diagram of the TL experimental setup



The transmission ratio  $T$  is given by

$$T = P_t/P_L \tag{2}$$

If the absorbance  $A$  is given by

$$A = 1 - T \tag{3}$$

Then we may write absorbed power  $P_f$  as

$$P_f = AP_L - P_{th}$$

In a completely fluorescence-quenched sample, the entire excitation energy is converted into non-radiative relaxation processes and hence the FQY,  $Q_f$  is given by [14]

$$Q_f = \frac{P_f \lambda_f}{AP_L \lambda} = \left(1 - \frac{P_{th}}{P_\alpha}\right) \frac{\lambda_f}{\lambda} \tag{4}$$

where  $P_\alpha = AP_L$ .

The ratio of peak fluorescence wavelength  $\lambda_f$  to the excitation wavelength  $\lambda$  takes account of the Stokes shift. Here  $P_{th}$  is directly proportional to the TL signal  $\eta$ , and  $P_\alpha$  is directly proportional to the TL signal  $\eta_\alpha$  corresponding to the concentration at which the fluorescence intensity is quenched completely. Thus, the quantum yield can be calculated by [14]

$$Q_f = \left(1 - \frac{\eta}{\eta_\alpha}\right) \frac{\lambda_f}{\lambda} \tag{5}$$

The TL signal  $\eta$  of the samples under study can be measured as the variation of light intensity at far field at the center of the probe beam.

#### 4 Results and discussion

The size of the AuNPs prepared using citrate reduction method is measured using transmission electron microscope (TEM, JEOL-JEM 2100) and the image is shown in Fig. 2. The inset shows the TEM image of an individual AuNP. The morphology of the particles is found to be nearly spherical with an average size of 15 nm. The absorption spectrum of the Au nanofluid is measured using

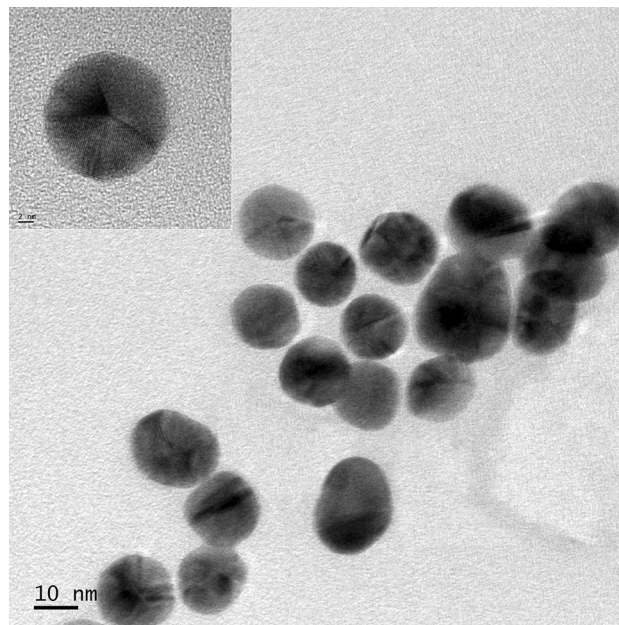


**Fig. 2** TEM image of the prepared AuNPs

a commercially available UV–VIS spectrophotometer (Shimadzu UV-2401 PC), and the normalized absorption spectrum of the prepared AuNPs is shown in Fig. 3. The spectrum shows the characteristic absorption band peaking around 520 nm, which can be attributed to the collective motion of electrons (surface plasmon resonance) of the gold atoms in the NP. The absorption spectrum remains the same even after 4 weeks of shelf-life of the colloids manifesting the stability as well as spherical nature of the particles in the fluid.

In the present study, we varied Rh6G concentration while retaining the AuNP concentration constant. The absorption spectra of Rh6G alone from  $0.3 \times 10^{-5}$  to  $0.3 \times 10^{-3}$  M are taken and are shown in Fig. 4. The values beyond  $0.5 \times 10^{-4}$  M are not shown here, as the absorbance values of dye molecules are beyond the detection limit of the instrument. In Rh6G, the phenyl group substitutes R in the main xanthene ring. The absorption band in the visible range for Rh6G corresponds

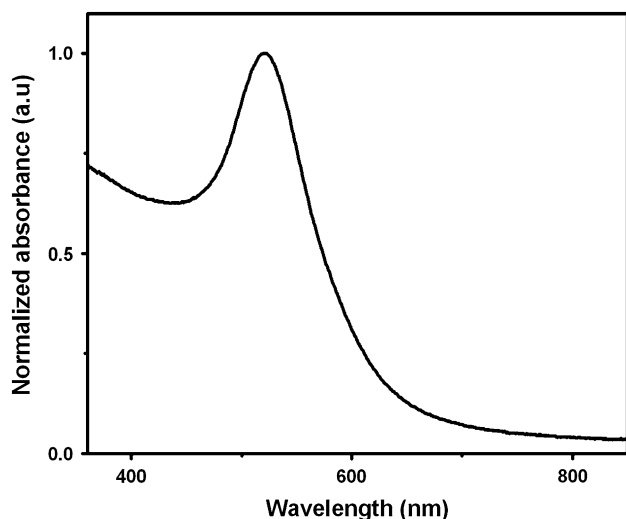


**Fig. 3** Normalized absorption spectrum of AuNPs

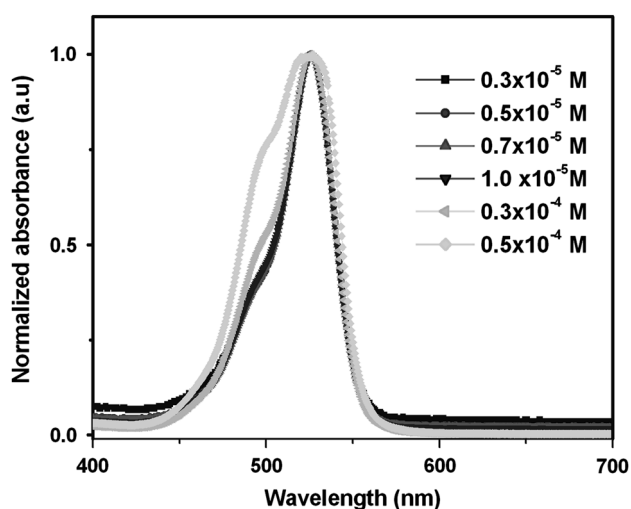


**Fig. 4** Normalized absorption spectra of various concentrations of Rh6G

to the transition moment largely parallel to the long axis of the molecule due to  $\pi - \pi^*$  transition. The absorption spectrum for  $0.5 \times 10^{-4}$  M Rh6G exhibits a peak around 525 nm that arises mainly from the monomer absorption and a shoulder around 498 nm indicating the presence of dimers. In aqueous medium, Rh6G forms stable ground-state dimers for higher concentrations via van der Waals dye-dye interaction or Rhodamine-water (counter ions) interactions.

In order to explore the influence of the prepared AuNPs on Rh6G, we carried out absorption spectral measurements for various concentrations of Rh6G (from  $0.3 \times 10^{-5}$  to  $0.3 \times 10^{-3}$  M) with a fixed concentration of NP solution (0.5 nM), in the range 400–900 nm. The corresponding normalized absorption spectra of the dye-NP mixture with

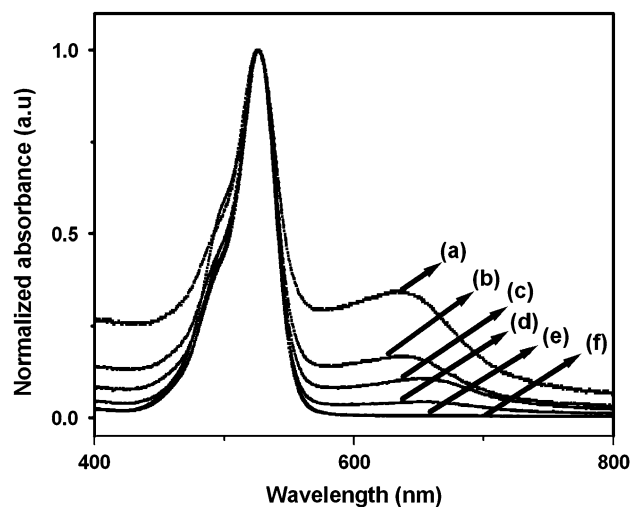


**Fig. 5** Normalized absorption spectra of Rh6G–AuNP mixture for various concentrations of Rh6G (a)  $0.3 \times 10^{-5}$ , (b)  $0.5 \times 10^{-5}$ , (c)  $0.7 \times 10^{-5}$ , (d)  $1.0 \times 10^{-5}$  (e)  $0.3 \times 10^{-4}$  and (f)  $0.5 \times 10^{-4}$  M

concentration of Rh6G varied from  $0.3 \times 10^{-5}$  to  $0.5 \times 10^{-4}$  M are shown in Fig. 5. The spectra of the mixture for Rh6G concentrations above  $0.5 \times 10^{-4}$  M are not shown as the absorbance values of dye molecules are beyond the detection limit of the instrument. From Fig. 5, it is clear that, compared to Rh6G alone which peak around 525 nm, the mixture absorption spectra shows additional spectral features peaking around 636, 637, 652 and 656 nm for concentrations  $0.3 \times 10^{-5}$ ,  $0.5 \times 10^{-5}$ ,  $0.7 \times 10^{-5}$  and  $1.0 \times 10^{-5}$  M, respectively. From Figs. 3 and 4, it is clear that there is a considerable spectral overlap between localized surface plasmon resonance (LSPR) band of nanoparticles and absorption band of the dye molecule. When the LSPR of the NP and absorption spectrum of the dye molecule are in resonance, there will be a strong coupling between large local electric field strength around the particle and molecular transition of the dye molecule. This near field coherent plasmonic-molecular resonance coupling between the Rh6G and AuNPs leads to the hybridization of the plasmonic and molecular resonances. Such coupling results in distinct spectral properties of the mixture compared to the superposition of constituents [19]. However, the additional spectral features in the present case are found to depend upon the dye concentration, as is evident from Fig. 5. In general, the citrate reduction approach to prepare nanoparticles results in the production of negatively charged NPs. The addition of a cationic dye such as Rh6G induces aggregation of negatively charged AuNPs leading to the formation of chain like agglomerated particles clusters of larger size [20, 21]. Interestingly, here, this effect is pronounced for lower dye concentration. The molecule induced particle aggregation is normally dominant for low concentration of dye molecules. When the dye

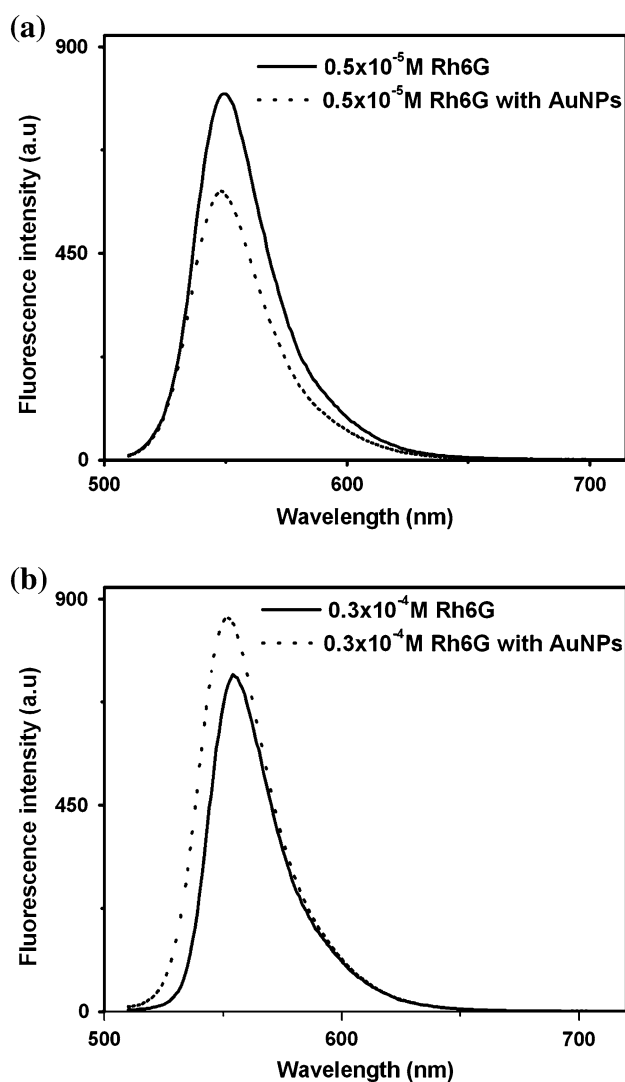


**Fig. 6** Fluorescence spectra of **a**  $0.5 \times 10^{-5}$  and **b**  $0.3 \times 10^{-4}$  M Rh6G in the presence and absence of AuNPs

concentration is higher than a threshold value, the dye molecules adsorbing the NPs inhibit the aggregation and add nothing to the absorption spectral features of the dye-NP mixture.

The fluorescence spectra for all dye concentrations (in the presence and absence of nanoparticles) are measured using the spectrofluorophotometer (Shimadzu RF-5301 PC) for an excitation wavelength of 500 nm. Figure 6a and b shows the fluorescence spectra of  $0.5 \times 10^{-5}$  and  $0.3 \times 10^{-4}$  M Rh6G in the presence and absence of gold nanoparticles. It is observed that the intrinsic fluorescence of dye-NP mixture is lower for low concentration of dye solution, whereas it exhibit high value for higher concentration of dye molecules. At lower concentration of the dye molecules, fluorescence quenching via non-radiative energy transfer between the dye molecules and NPs/aggregates dominates. At higher concentrations, the dye

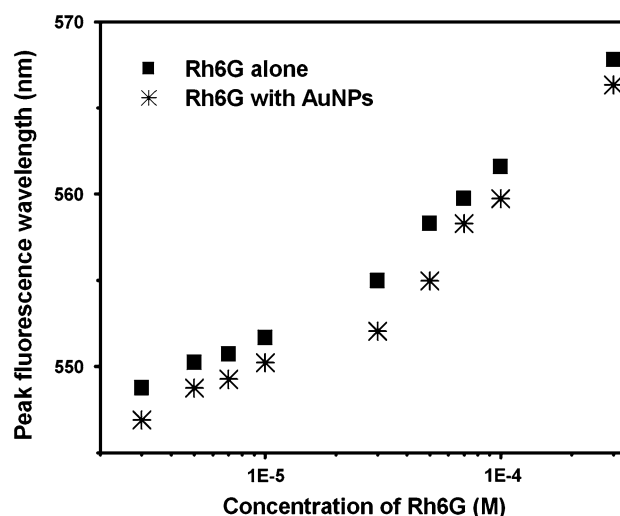


**Fig. 7** Variation of peak fluorescence wavelength with concentration of Rh6G in the presence and absence of AuNPs

molecules adsorbed around the nanoparticles prevent the aggregation of NPs as well as reduce the possibility of dimer formation of dye molecules. This results in an enhanced fluorescence signal in the presence of nanoparticles. Additionally, the steady-state fluorescence studies show a blue shift in fluorescence spectral peak. The variation of peak fluorescence wavelength of Rh6G with and without the presence of AuNPs in the concentration range from  $0.3 \times 10^{-5}$  to  $0.3 \times 10^{-3}$  M is shown in Fig. 7. In general, for Rh6G in water, the monomer fluorescence dominates over the dimer fluorescence. The redshift in the fluorescence peak of Rh6G with increase in dye concentration is quiet well known and arise as a consequence of secondary absorption effects due to the overlap between the emission spectrum of the dye and low energy tail of its absorption band. Additionally, other dynamic process such as energy loss due to dissipation of vibration energy, reorientation of solvent molecules around the excited state dipole, specific interaction between the fluorophore and the solvent or solute can contribute to the observed redshift [22]. Interestingly, the presence of AuNPs results in blue shift to the emission peak corresponding to each dye concentration. This can be attributed to change in local environment of emitting molecules. A nonpolar environment with the addition of NPs causes blue shift in the peak emission wavelength. In addition, the H-type aggregation of dye molecules that adsorb on the NP surface also may contribute to the observed blue shift. Moreover, lack of additional spectral features in the fluorescence spectra indicates that H-type aggregation (where the molecules form perfect sandwich structures) is dominant in our case compared to J-type aggregates (with perfect 'end-to-end' alignment of dipole moment) [23].

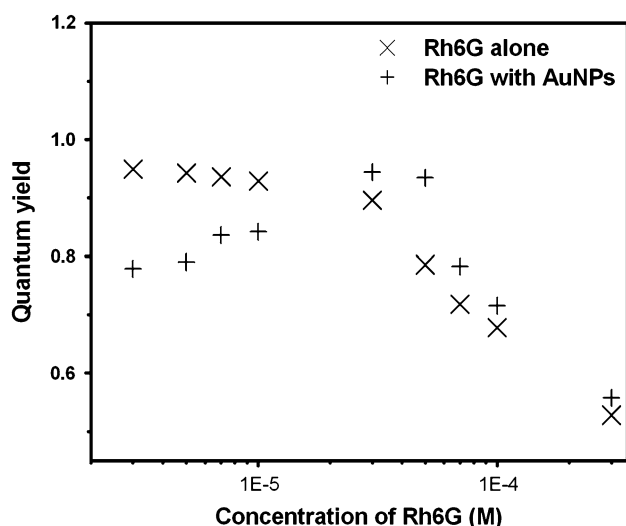
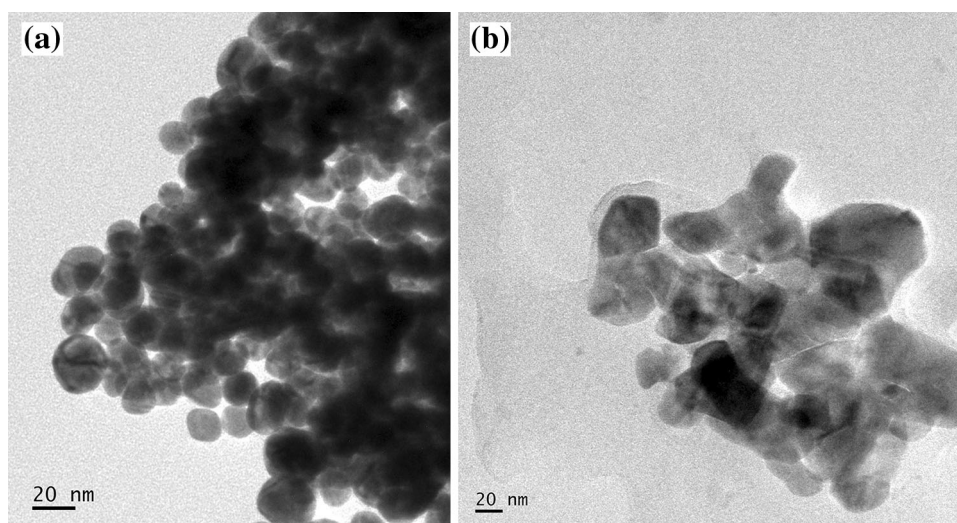


**Fig. 8** Variation of FQY with concentration of Rh6G in the presence and absence of AuNPs

The FQY of pure dye and the dye-nanoparticle mixture as a function of Rh6G concentrations ranging from  $0.3 \times 10^{-5}$  to  $0.3 \times 10^{-3}$  M is calculated using Eq. (5) and is shown in Fig. 8. It is clear from Fig. 8 that pure dye molecules exhibit a FQY value nearly equal to reported value for low concentration of the dye molecules and for concentrations beyond  $0.3 \times 10^{-4}$  M, FQY shows a sharp decrease [14]. This can be understood in terms of formation of ground-state dimers and trimers in aqueous solution of Rh6G. For Rh6G dissolved in water, the dimer binding energy is greater than  $kT$  [24], so that ground-state dimers are stable at room temperature. In water, H and J class of dimer can be formed with former as dominant fraction. H class of dimer is thought as nonfluorescing, and the J class of dimer is weakly fluorescing [12]. Moreover, the

formation of dimers at higher concentrations of dye results in a competition between increasing dimer absorption and decreasing monomer absorption. This results in drastic reduction in FQY with increase in dye concentration. In the presence of AuNPs, the fluorescence of Rh6G exhibits a different concentration-dependent FQY behavior. At lower concentration of Rh6G, the FQY of the dye-NP mixture is lower than the corresponding concentration in which dye alone is present and it increases with increase in dye concentration. However, for concentrations higher than  $1 \times 10^{-5}$  M, the dye-NP mixture FQY follows the similar behavior as corresponding dye concentration. It is worth to note here that the FQY value of dye-NP mixture for concentrations higher  $1 \times 10^{-5}$  M is slightly greater than corresponding dye concentrations. At very low concentration of dye molecules ( $0.3 \times 10^{-5}$ – $1.0 \times 10^{-5}$  M), the introduction of NPs into the mixture results in fluorescence quenching. In the vicinity of a NP, the strong plasmon field around the NP can influence emission behavior of the dye molecule, depending upon the distance between the metal core and dye molecule. It has been reported that dye-NP interaction is effective up to 22 nm, and it is better explained in terms of nanomaterial surface energy transfer rather than Froster energy transfer mechanism between the dipoles that is effective up to 10 nm. Recent studies showed that this energy transfer mechanism follows a distance dependence of  $1/d^4$  compared to  $1/d^6$  dependence of dipole-dipole energy transfer mechanism in dye mixtures [25–28]. The non-radiative energy transfer between the dye molecule and NP depends upon the spectral overlap between the emission spectra of dye molecule (donor) and the absorption spectrum of the NP (acceptor). As explained above, the non-radiative energy transfer quenches the fluorescence of emitter and results in reduced FQY. In addition, in aqueous solutions, the cationic Rh6G

**Fig. 9** TEM images of the gold nanoparticles in **a**  $0.3 \times 10^{-5}$  and **b**  $0.7 \times 10^{-4}$  M Rh6G



molecules tend to cluster around the negatively charged AuNPs through the electrostatic interaction. The adsorption of dye molecules around the NPs results in surface charge neutralization and renders the coalescence of the NPs [29]. These clustered NPs acts as more efficient quencher due to enhanced metal surface area and hence decrease the FQY values of the dye. The physical adsorption of dye molecules at higher concentration results in the formation of a dielectric shell around the NPs. Such a shell formation around the NP can cause a change in local dielectric environment of the NP and can cause spectral shift in the plasmonic absorption band of the NP [30]. Once a monolayer of the shell is formed around the NP, the quenching efficiency of the NPs is reduced due to decreased aggregation and results in an increase in FQY of the dye-NP mixture. In order to validate these assumptions, TEM images of the NPs at lower and higher concentration of dye are taken and are shown in Fig. 9a and b. The TEM images indicate that aggregation of NPs occurs for lower concentration of dye molecules whereas dimer formation dominates at higher concentrations. This observation is consistent with the absorption spectral measurement shown in Fig. 5, where the additional spectral features due to aggregation of NPs become less prominent and the influence of dimer formation becoming more and more evident. Thus, at very high concentration, the quenching due to dimer formation dominates rather than NP induced quenching. A slight enhanced FQY value of dye-NP mixture compared to dye alone at very high concentration may be due to reduced dimer formation in the presence of NPs.

## 5 Conclusions

To summarize, the dye concentration have pronounced influence on the absorption and emission behavior of dye-nanoparticle mixture. At lower concentrations, a cationic dye such as Rhodamine 6G causes aggregation of negatively charged gold nanoparticle and results in additional absorption spectral features of the pure dye. As the dye concentration increases in the dye-NP mixture, a monolayer formed due to the adsorption of the dye molecules around the nanoparticles inhibits the aggregation of nanoparticles and results in an enhancement of the fluorescence signal as well as the quantum yield. At very high concentration, the well-known dimer formation of dye molecules result in reduced value of the quantum yield. This is manifested in a non-monotonic behavior of the concentration-dependent fluorescence quantum yield of the dye-nanoparticle mixture. Additionally, the introduction of nanoparticles into the dye solution causes a blue shift in the peak fluorescence wavelength due to dye-NP interaction. The thermal-lens studies clearly showed that the

nanoparticles reduce the quantum efficiency values when the concentration of dye molecules is low via non-radiative energy transfer mechanism. At higher concentration of dye molecules, the nanoparticles decrease direct interaction of the dye molecules and reduce the possibility of dimer formation. The present study enables to conclude that the concentration of dye molecules is extremely important while considering the potential applications of dye-nanoparticle mixtures.

## References

1. D.K. Lim, K.S. Jeon, J.H. Hwang, H. Kim, S. Kwon, Y.D. Suh, J.M. Nam, *Nat. Nanotechnol.* **6**, 452 (2011)
2. C.M. MacLaughlin, N. Mullaithilaga, G. Yang, S.Y. Ip, C. Wang, G.C. Walker, *Langmuir* **29**, 1908 (2013)
3. M. Iosin, P. Baldeck, S. Astilean, *Nucl. Instrum. Methods Phys. Res. Sect. B* **267**, 403 (2009)
4. M.A. Noginov, G. Zhu, A.M. Belgrave, R. Bakker, V.M. Shalaev, E.E. Narimanov, S. Stout, E. Herz, T. Suteewong, U. Wiesner, *Nature* **460**, 1110 (2009)
5. K.A. Kang, J. Wang, J.B. Jasinski, S. Achilefu, *J. Nanobiotechnol.* **9**, 16 (2011)
6. C. Würth, M.G. González, R. Niessner, U. Panne, C. Haisch, U.R. Genger, *Talanta* **90**, 30 (2012)
7. B.R. Kumar, N.S. Basheer, S.D. George, A. Kurian. *Photonics (ICP), 3rd International Conference on. IEEE*, **149** (2012)
8. N.S. Basheer, B.R. Kumar, A. Kurian, S.D. George, *J. Lumin.* **137**, 225 (2013)
9. A. Kurian, K.P. Unnikrishnan, P. Gopinath, V.P.N. Nampoori, C.P.G. Vallabhan, *J. Nonlinear Opt. Phys. Mat.* **10**, 415 (2001)
10. A. Kurian, S.D. George, V.P.N. Nampoori, C.P.G. Vallabhan, *Spectrochim. Acta Part A* **61**, 2799 (2005)
11. A. Kurian, S.D. George, C.V. Bindhu, V.P.N. Nampoori, C.P.G. Vallabhan, *Spectrochim. Acta A* **67**, 678 (2007)
12. C.V. Bindhu, S.S. Harilal, V.P.N. Nampoori, C.P.G. Vallabhan, *Mod. Phys. Lett. B* **13**, 563 (1999)
13. J.H. Brannon, D. Magde, *J. Phys. Chem.* **82**, 705 (1978)
14. A. Santhi, M. Umadevi, V. Ramakrishnan, P. Radhakrishnan, V.P.N. Nampoori, *Spectrochim. Acta Part A* **60**, 1077 (2004)
15. A. Kurian, S.T. Lee, K.P. Unnikrishnan, D.S. George, V.P.N. Nampoori, C.P.G. Vallabhan, *J. Nonlinear Opt. Phys. Mat.* **12**, 75 (2003)
16. A. Santhi, U.L. Kala, R.J. Nedumpara, A. Kurian, M.R.P. Kurup, P. Radhakrishnan, V.P.N. Nampoori, *Appl. Phys. B* **79**, 629 (2004)
17. C.V. Bindhu, S.S. Harilal, G.K. Varier, R.C. Issac, V.P.N. Nampoori, C.P.G. Vallabhan, *J. Phys. D Appl. Phys.* **29**, 1074 (1996)
18. G. Frens, *Nat. Phys. Sci.* **241**, 20 (1973)
19. H. Chen, T. Ming, L. Zhao, F. Wang, L.D. Sun, J. Wang, C.H. Yan, *Nano Today* **5**, 494 (2010)
20. E.O. Ganbold, J.H. Park, U. Dembereldorj, K.S. Ock, S.W. Joo, *J. Raman Spectrosc.* **42**, 1614 (2011)
21. J. Zhu, H.W. Gao, J. Li, J.W. Zhao, *Plasmonics* **8**, 1003 (2013)
22. A. Kurian, N.A. George, B. Paul, V.P.N. Nampoori, C.P.G. Vallabhan, *Laser Chem.* **20**, 99 (2002)
23. R. Sasai, N. Iyi, T. Fujita, F.L. Arbeloa, V.M. Martínez, K. Takagi, H. Itoh, *Langmuir* **20**, 4715 (2004)
24. A. Penzkofer, W. Leupacher, *J. Lumin.* **37**, 61 (1987)
25. M.P. Singh, G.F. Strouse, *J. Am. Chem. Soc.* **132**, 9383 (2010)

26. T.L. Jennings, M.P. Singh, G.F. Strouse, *J. Am. Chem. Soc.* **128**, 5462 (2006)
27. T. Sen, S. Sadhu, A. Patra, *Appl. Phys. Lett.* **91**, 043104 (2007)
28. K.K. Haldar, T. Sen, A. Patra, *J. Phys. Chem. C* **112**, 11650 (2008)
29. N. Chandrasekharan, P.V. Kamat, J. Hu, G. Jones, *J. Phys. Chem. B* **104**, 11103 (2000)
30. J. Zhu, K. Zhu, L. Huang, *Phys. Lett. A* **372**, 3283 (2008)